Nuclear condensation and symmetry energy of dilute nuclear matter: An *S*-matrix approach

J. N. De* and S. K. Samaddar†
Theory Division, Saha Institute of Nuclear Physics, 1/AF Bidhannagar, Kolkata 700064, India
(Received 30 September 2008; published 30 December 2008)

Based on the general analysis of the grand canonical partition function in the *S*-matrix framework, the calculated results on symmetry energy, free energy, and entropy of dilute warm nuclear matter are presented. At a given temperature and density, the symmetry energy or symmetry free energy of the clusterized nuclear matter in the *S*-matrix formulation deviates, particularly at low temperature and relatively higher density, in a subtle way, from the linear dependence on the square of the isospin asymmetry parameter $X = (\rho_n - \rho_p)/(\rho_n + \rho_p)$, contrary to those obtained for homogeneous nucleonic matter. The symmetry coefficients, in conventional definition, can then be even negative. The symmetry entropy similarly shows a very different behavior.

DOI: 10.1103/PhysRevC.78.065204 PACS number(s): 21.65.Ef, 12.40.Ee, 21.65.Mn, 24.10.Pa

I. INTRODUCTION

Understanding properties of symmetry energy for low density nuclear matter is of much topical interest in both astrophysical and laboratory contexts. The supernova simulation dynamics have a sensitive dependence on the symmetry energy [1]; a higher symmetry energy, for example, leads to a lower electron (e^-)-capture rate in the supernova collapse phase that may result in a stronger explosive shock. The variations in the e^--capture rate also produce changes in the neutrino luminosities that are potentially observable. The isotopic abundance of relatively heavier elements in explosive nucleosynthesis is further directly correlated to the symmetry energy. The neutron skin thickness of heavy nuclei also has a direct dependence on the density variation of the symmetry energy [2,3]. At subnormal densities ($0.2 \leqslant \rho/\rho_0 \leqslant 1.0$, ρ_0 is the saturation density of nuclear matter), the symmetry coefficients that are a measure of the symmetry energy per baryon ($e_{\rm sym}$) have recently been estimated from analysis of data related to isotopic distributions [4], isospin diffusion [5,6], and isoscaling [7,8] in heavy ion reactions. The different analyses give somewhat different results. In the density domain mentioned, the symmetry coefficient $C_E(= e_{\rm sym}/X^2)$ varies with density as $C_E(\rho) \sim C_E(\rho_0)(\rho/\rho_0)^\gamma$ with γ lying in a broad range [8,9], between 0.55 and 1.05. A more definitive answer to the question of the density dependence of symmetry energy is still wanting.

On the theoretical side, symmetry energy of infinite nuclear matter has been calculated over a wide density range in many guises; many-body theories using various nucleon-nucleon interactions or interaction Lagrangians [9] have lead to varying results [10]. There have also been some recent investigations on the symmetry free energy of hot nuclear matter [11] and also of finite nuclei [12]. These calculations differ in details, but the general qualitative behavior of the symmetry coefficients with density do not deviate much from the experimental trend. A similar power law variation is exhibited; the exponent γ lies mostly within the broad limits as extracted from experimental analyses.

The above calculations have been done in the mean-field (MF) approximation; the system is taken to be homogeneous nucleonic matter. For dilute nuclear matter, however, the system minimizes its total energy or free energy by forming clusters [13,14]. A detailed knowledge of the composition of nuclear matter is then needed to appreciate how the symmetry energies are affected when matter gets clusterized. This has a direct role in a better understanding of neutrino-driven energy transfer in inhomogeneous supernova matter [15]. Using the virial expansion technique, clusterization in dilute nuclear matter and its import in the evaluation of the symmetry coefficients has been investigated recently by Horowitz and Schwenk [16] where they considered the matter to be composed of n, p, α. Investigations with the same cluster species have been followed further [17] to connect experimentally the temperature and density-dependent entropic contributions to the symmetry free energy coefficient. The resulting symmetry coefficients are found to be considerably larger than the corresponding ones obtained from MF calculations. This is an important result; it shows the strong role of clusterization and naturally calls for a realization of symmetry coefficients if all possible permissible clusters are incorporated in the calculation. The present article is an attempt in this direction.

II. ELEMENTS OF THEORY

The grand canonical partition function in the *S*-matrix formalism of statistical mechanics proposed by Dashen, Ma, and Bernstein [18] sets the logical framework of our calculation. The details of the formalism as applied to nuclear matter are given in Ref. [19]; for the sake of completeness, the essentials are presented in the following.

The partition function $\mathcal{Z}$ for the two-component nuclear matter composed of the elementary species neutrons and protons is written as

$$\mathcal{Z} = \mathrm{Tr}\, e^{-\beta(H-\mu_p\hat{N}_p-\mu_n\hat{N}_n)}, \tag{1}$$

where β is the inverse of temperature T of the system, H the total Hamiltonian, $\hat{N}_{p,n}$ are the number operators for protons and neutrons, and $\mu_{p,n}$ are the corresponding chemical

*jn.de@saha.ac.in
†santosh.samaddar@saha.ac.in

potentials. The partition function can be decomposed as

$$\mathcal{Z} = \sum_{Z,N=0}^{\infty} \zeta_p^Z \zeta_n^N \, \mathrm{Tr}_{Z,N} \, e^{-\beta H}, \tag{2}$$

where the fugacities are given by $\zeta_p = e^{\beta\mu_p}$, $\zeta_n = e^{\beta\mu_n}$. The trace $\mathrm{Tr}_{Z,N}$ is taken over states of Z protons and N neutrons. For small ζ_p and ζ_n, the quantity $\ln \mathcal{Z}$ can be expanded in a virial series,

$$\ln \mathcal{Z} = {\sum_{Z,N}}' D_{Z,N} \zeta_p^Z \zeta_n^N. \tag{3}$$

The prime on Σ indicates that the term with $Z = N = 0$ is excluded. Evaluation of the virial coefficients $D_{Z,N}$ gives the partition function and thence the thermodynamic behavior of the system.

Following the temperature-Green's function method, it was shown in Ref. [18] that all the dynamical information concerning the microscopic interaction in the grand potential of the system can be collected in two types of terms so that the partition function is written as

$$\ln \mathcal{Z} = \ln \mathcal{Z}^{(0)}_{\mathrm{part}} + \ln \mathcal{Z}_{\mathrm{scat}}. \tag{4}$$

The first term corresponds to contributions from stable single-particle states of clusters of different sizes (neutrons and protons included) formed in the infinite system behaving like an ideal quantum gas [the superscript (0) indicates this behavior] and the second term corresponds to contribution from multiparticle scattering states, respectively. The particle piece can further be split into contributions from ground states and excited states of the bound nucleon clusters, so that

$$\ln \mathcal{Z}^{(0)}_{\mathrm{part}} = \ln \mathcal{Z}^{(0)}_{\mathrm{gr}} + \ln \mathcal{Z}^{(0)}_{\mathrm{ex}}. \tag{5}$$

The first term in Eq. (5) is a sum of ideal gas terms, one for each of the ground states of all the possible species of mass A with Z protons and N neutrons that can be formed in the system,

$$\ln \mathcal{Z}^{(0)}_{\mathrm{gr}} = \mp V \sum_{Z,N} g \int \frac{d^3p}{(2\pi)^3} \times \ln\left(1 \mp \zeta_{Z,N} e^{-\beta(p^2/2Am)}\right). \tag{6}$$

Here m is the nucleon mass, p is the momentum of the nucleus, and $\zeta_{Z,N}$ is the "effective fugacity" given by $\zeta_{Z,N} = e^{\beta(\mu_{Z,N} + B_{Z,N})}$. $B_{Z,N}$ is the binding energy of the nucleus and $\mu_{Z,N}$ is its chemical potential. From the condition of chemical equilibrium among the different species, $\mu_{Z,N} = Z\mu_p + N\mu_n$.

The $\mp$ sign in Eq. (6) corresponds to nuclei with A even or odd, obeying Bose or Fermi statistics, V is the volume of the system, and g is the spin degeneracy. The sum includes the original elementary species, namely, the neutrons and protons. The Coulomb interaction is assumed absent in nuclear matter; ideally the sum in Eq. (6) would involve infinite terms as the maximum cluster mass A can then even be infinite. However, for applications to real physical systems such as neutron star matter, the Coulomb effect is to be included in the binding energies of nuclei. In that case, the sum is finite, conditioned by the stability of nuclei with inclusion of Coulomb in the binding energies. Calculations in the S-matrix formalism with inclusion of Coulomb in the fragment binding energies will henceforth be referred to as SMF; those without Coulomb will be called SNC. Equation (6) can be readily expanded in a virial series as

$$\ln \mathcal{Z}^{(0)}_{\mathrm{gr}} = V \sum_{Z,N} \frac{g}{\lambda^3(Am)} \left(\zeta_{Z,N} \pm \frac{\zeta^2_{Z,N}}{2^{5/2}} + \cdots\right), \tag{7}$$

in powers of effective fugacities provided $|\zeta_{Z,N}| < 1$. Here, $\lambda(Am) = \sqrt{2\pi/(AmT)}$ is the thermal wavelength of a cluster of mass Am. We work in natural units $\hbar = c = 1$. A nucleus in a particular excited state is taken as a distinctly different species and can be treated in the same footing as the ground state. The density of states is quite high in relatively heavy nuclei and increases nearly exponentially with the square root of excitation energy E and so the contribution of the excited states of a single nucleus is written as an integral over E of the ideal gas term weighted with the level density $\omega(A, E)$,

$$\ln \mathcal{Z}^{(0)}_{\mathrm{ex}} = \mp V {\sum_{Z,N}}' g \int_{E_0}^{E_s} dE\, \omega(A, E) \times \int \frac{d^3p}{(2\pi)^3} \ln\left(1 \mp \zeta_{Z,N} e^{-\beta(p^2/2Am+E)}\right). \tag{8}$$

For the level density, we take the expression [20]

$$\omega(A, E) = \frac{\sqrt{\pi}}{12a^{1/4}} \frac{e^{2\sqrt{aE}}}{E^{5/4}}. \tag{9}$$

The level density parameter a is taken as $A/8$ MeV^{-1}, its empirical value.

In Eq. (8), the prime on Σ denotes exclusion of the light nuclei ($A \leqslant 8$) from the sum. For these nuclei, we take only the ground states; their degeneracy factor g is taken from experiments. For other nuclei, for both ground and excited states, g is taken as 1 or 2, according as they are bosonic or fermionic. The lower limit E_0 is dictated by the location of the first excited state. The upper limit E_s is the separation energy. We take $E_0 = 2$ MeV and $E_s = 8$ MeV.

The scattering piece $\ln \mathcal{Z}_{\mathrm{scat}}$ of Eq. (4) can be formally, but explicitly, written [19] for nuclear matter as

$$\ln \mathcal{Z}_{\mathrm{scat}} = V \sum_{Z_t,N_t} \frac{e^{\beta\mu_{Z_t,N_t}}}{\lambda^3(A_t m)} \sum_{\sigma} e^{\beta B_{Z_t,N_t,\sigma}} \int_0^{\infty} d\epsilon\, e^{-\beta\epsilon} \times \frac{1}{2\pi i} \mathrm{Tr}_{Z_t,N_t,\sigma} \left(\mathcal{A} S^{-1}(\epsilon) \frac{\partial}{\partial\epsilon} S(\epsilon)\right)_c. \tag{10}$$

Here, the double sum refers to the sum over all possible scattering channels, each having its chemical potential μ and formed by taking any number of particles from any of the stable species (proton, neutron, and nuclei in their ground and excited states) and the trace is over all plane wave states for each of these channels. S is the scattering operator and $\mathcal{A}$ the boson symmetrization or fermion antisymmetrization operator. The subscript c denotes only the connected parts in the diagrammatics of the expression in the parentheses. A channel in the set has a total number of Z_t protons and N_t neutrons ($A_t = N_t + Z_t$); σ denotes all other labels required to fix a channel within this set. $B_{Z_t,N_t,\sigma}$ is the sum of the individual

binding energies of all the particles in the channel and ϵ is the total kinetic energy in the c.m. frame of the scattering partners. Examination of Eq. (10) shows that channels with larger binding energies are more important, because of the factor $e^{\beta B_{Z_t,N_t,\sigma}}$. Furthermore, two-particle channels are expected to dominate over multiparticle channels with the same Z_t and N_t from binding energy consideration. We therefore consider only two-particle scattering channels. It is convenient to divide the channels into light ones, consisting of low mass particles ($A < 8$, say) and heavy ones ($A \geqslant 8$), so that we write

$$\ln \mathcal{Z}_{\rm scat} = \ln \mathcal{Z}_{\rm light} + \ln \mathcal{Z}_{\rm heavy} \tag{11}$$

as the sum of contributions from the light and heavy channels.

Experimentally it is known that the scattering of relatively heavier nuclei is dominated by a multitude of resonances near the threshold. The S-matrix elements are then approximated by resonances. Following Refs. [21] and [22], each of these resonances are treated like an ideal gas term and then $\ln \mathcal{Z}_{\rm heavy}$ can be written in the same form of $\ln \mathcal{Z}^{(0)}_{\rm ex}$, assuming their level density to be the same as those of the excited states. The integration over E in Eq. (8) now extends from E_s to E_r, the limit of resonance domination. The damping of the integral in Eq. (10) due to the presence of the Boltzmann factor assures contribution only from low energies; we therefore take $E_r \simeq 12$ MeV.

The scattering channels $NN, Nt, N\ {\rm He}^3, N\alpha$ (N refers to nucleon), and $\alpha\alpha$ are considered for evaluation of $\mathcal{Z}_{\rm light}$. Inclusion of other light particle scattering channels may have some influence on the present results. In intermediate energy heavy ion collisions, for example, deuteron usually has considerable multiplicity and the contribution to $\ln \mathcal{Z}_{\rm light}$ from deuteron scattering channels is worth further exploration. With the choice of the scattering channels as mentioned above, we then write

$$\ln \mathcal{Z}_{\rm light} = \ln \mathcal{Z}_{NN} + \ln \mathcal{Z}_{Nt} + \ln \mathcal{Z}_{N{\rm He}^3} + \ln \mathcal{Z}_{N\alpha} + \ln \mathcal{Z}_{\alpha\alpha}. \tag{12}$$

We explicitly write the contribution from the NN channel. If we consider only elastic two-body scattering, the trace in Eq. (10) becomes a sum over the derivative of the phase shifts of the appropriate partial waves. It gives formulas of the same form as derived by Beth and Uhlenbeck [23] for the second virial coefficient. It is given as

$$\ln \mathcal{Z}_{NN} = \frac{V}{\lambda^3(2m)}\left\{\left(\zeta_p^2 + \zeta_n^2\right)\Delta_{NN}^{I=1} + \zeta_p\zeta_n\left(-3 + \Delta_{NN}^{I=1} + \Delta_{NN}^{I=0}\right)\right\}. \tag{13}$$

Here I is the isospin index and

$$\Delta_{NN}^{I} = \frac{1}{\pi T}\int_0^\infty d\epsilon e^{-\beta\epsilon}\sum_{S,L,J}(2J+1)\delta^{NN}_{^{2S+1}L_J}(\epsilon). \tag{14}$$

The quantity $\delta^{NN}_{^{2S+1}L_J}(\epsilon)$ refers to the NN phase shift in the LSJ channel. The contributing partial waves are determined by I through the requirement of antisymmetry on the total wave function of the NN system. The other terms in Eq. (12) have nearly similar forms [19]. The Δ's for the NN, $N\alpha$, and $\alpha\alpha$ channels are evaluated in Ref. [16] and those for N $\rm He^3$ and Nt are available in Ref. [24]. This completes the evaluation of partition function for nuclear matter. It is then straightforward to get the relevant observables like the pressure P, the number density of the ith species ρ_i, the free energy per baryon f, or the entropy per baryon s from the relations

$$P = T\frac{\ln \mathcal{Z}}{V}, \quad \rho_i = \zeta_i\left(\frac{\partial}{\partial\zeta_i}\frac{\ln \mathcal{Z}}{V}\right)_{V,T},$$
$$f = \frac{1}{\rho}\left(\sum_i \mu_i\rho_i - P\right), \quad s = \frac{1}{\rho}\left(\frac{\partial P}{\partial T}\right)_{\mu_i}, \tag{15}$$

with the baryon density $\rho = \sum_i A_i\rho_i$.

III. RESULTS AND DISCUSSION

We have calculated the nuclear equation of state (EOS), the fragment distributions, the symmetry free energy, the symmetry entropy, and the symmetry coefficients (symmetry energy coefficient C_E and the symmetry free energy coefficient C_F) for dilute nuclear matter. The calculations have been done in the SMF and the SNC model where all possible nuclear species are considered and compared, to explore the role of heavy species, with calculations [16,24] where only the light species (n, p, d, t, $\rm He^3$, and α) are taken into account. The latter model is subsequently referred to as the light species model (LSM). The three models (SMF, SNC, and LSM) are collectively referred to as the condensation models. To highlight the importance of clusterization on the physical observables, the MF results are also presented.

In practice, an asymptotic wave function may not have a precise meaning at relatively high density; it would then be difficult to have a meaningful expression of the partition function in terms of the S-matrix elements. We, therefore, restrict our calculations to low density nuclear matter and have considered up to a baryon density $\rho = 0.01$ fm^{-3}.

In Fig. 1, the EOS ($P - \rho$) are displayed for symmetric nuclear matter ($\rho_n = \rho_p$) at temperatures $T = 2$, 4, and

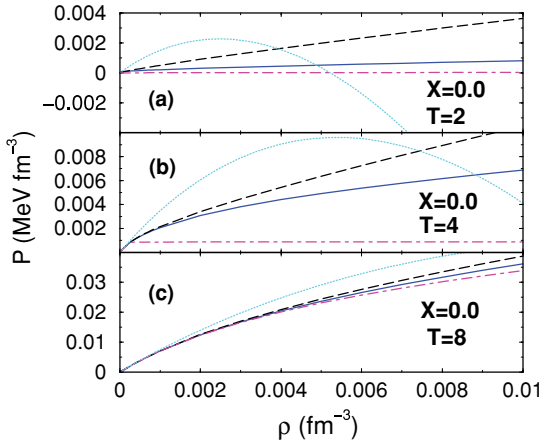

FIG. 1. (Color online) EOS for symmetric nuclear matter at $T =$ 2, 4, and 8 MeV. Calculations are shown for models in mean-field (dotted cyan), LSM (dashed black), SNC (dot-dashed magenta), and SMF (solid line, blue).

8 MeV. The dotted lines refer to calculations in the MF model with the SkM* interaction. At low temperatures, it is seen that the system enters the unphysical region ($dP/d\rho < 0$) in the density range considered. This can be avoided by applying Maxwell's construction. In the SMF, because of the many-body correlations (condensation), this unphysical behavior does not arise. Because Coulomb interaction is absent in nuclear matter, to compare results from the mean field, a set of S-matrix calculations has been carried out with Coulomb switched off in the nuclear binding energies (SNC). The SNC calculations are represented in the figure as dot-dashed lines. With isothermal compression, at lower temperatures, the pressure levels off at very low densities as shown by the dot-dash lines in Figs. 1(a) and 1(b), signaling a behavior like a first-order phase transition. At the higher temperature 8 MeV, the said transition starts at a density beyond 0.01 fm^{-3}; it is not seen in the figure. The sum in Eq. (3) for the SNC calculation runs up to infinity in principle; in practice, one takes a finite sum for calculational facilitation. We have taken the maximum mass $A_{\max} = 1000$. The results are found to be not very sensitive to further increase of $A_{\max}$ [25]. The binding energies of these nuclei are obtained using a simple liquid-drop mass formula [26] with Coulomb switched off.

To help comparison with physical systems such as neutron star matter, we have also considered phenomenological binding energies (Coulomb included) [27] of the nuclei that limit the number of terms in the sum to ∼9000 nuclei in their ground states with $A_{\max} = 339$ and $Z_{\max} = 136$. The EOS in the SMF are shown by the full lines. It is seen that with Coulomb in the binding energies, the signature of the first-order phase transition is washed out with monotonic increase in pressure on isothermal compression. The results in the LSM model are shown by the dashed lines. At a given density, in the SMF, the fragment multiplicity is comparatively less as more nucleons get bound in larger clusters; the pressure is also then less compared to the LSM model. The deviations are significant, particularly at higher density and at lower temperature.

The composition of matter at different densities and temperatures for symmetric nuclear matter is shown in Fig. 2 through the charge multiplicities. The left, middle, and right panels correspond to temperatures $T = 2$, 4, and 8 MeV, respectively, at three different baryon densities, $\rho = 0.0001$, 0.001, and 0.01 fm^{-3}. The solid lines display the results from the SMF model, the dashed lines are the ones from the LSM model, and the dot-dashed lines correspond to the ones from the SNC model. Examination of the results brings out a few important findings: (i) At very low densities, the multiplicities up to $Z = 2$ are practically the same in the SMF and LSM models. In the SMF model, heavier fragments may be formed, but that is insignificant. (ii) With increase in density, heavy fragment formation can no longer be neglected. Increase in temperature hinders the heavy cluster formation. The multiplicity distributions display a saw-toothed nature. This is an odd-even effect due to inclusion of pairing in the phenomenological binding energies of the nuclear clusters; this effect is diluted with an increase in temperature. (iii) At relatively low temperatures and higher densities, in the SNC model, the matter consists of only nucleons and very heavy nuclei; the matter resembles liquid-like structures along with a negligible fraction of nucleonic gas. These features are observed at all the three densities at $T = 2$ MeV and at $\rho = 0.01$ fm^{-3} for $T = 4$ MeV. These results are not shown in the figure. With increasing temperature and decreasing density, the liquid-like structures disappear. These features appear from a delicate dependence of the chemical potential on the density and temperature and the dependence of fragment binding energy on increasing fragment mass, which tends to saturate at ∼16 MeV per nucleon.

The evolution of symmetry free energy per baryon $f_{\rm sym}$ as a function of asymmetry X^2 at different temperatures and densities is displayed in Fig. 3. The symmetry free energy for a given density and temperature is defined as

$$f_{\rm sym} = f(X) - f(0) + \frac{1}{\rho}\sum_i [\rho_i(X) - \rho_i(0)]B_c^i, \quad (16)$$

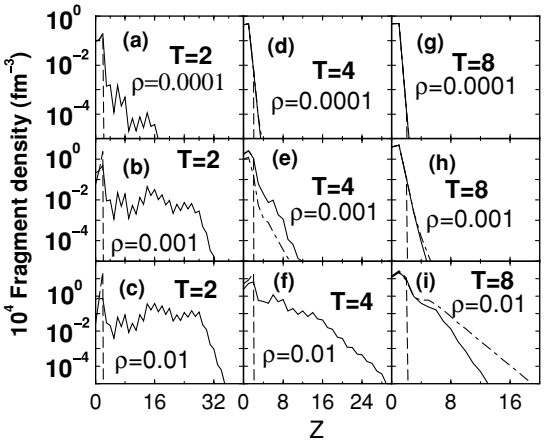

FIG. 2. The charge distributions at different temperatures and densities are compared in the models of LSM (dashed line), SNC (dot-dashed), and SMF (full line).

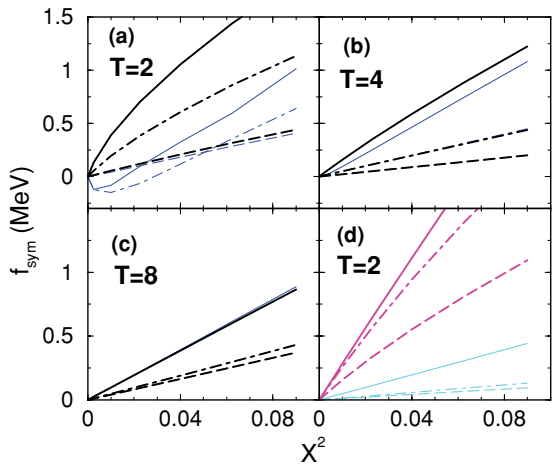

FIG. 3. (Color online) The symmetry free energy shown as a function of X^2 at different temperatures. The dashed, dot-dashed, and solid lines correspond to $\rho = 0.0001$, 0.001, and 0.01 fm^{-3}, respectively. The results are calculated in the models of the mean field (thin cyan), LSM (thick black), SNC (thick magenta), and the SMF (thin blue).

where B_c^i is the Coulomb contribution to the binding energy of the ith fragment species. The symmetry energy $e_{\rm sym}$ can be defined likewise. The dashed, dot-dashed, and solid lines correspond to calculations at densities of $\rho = 0.0001$, 0.001, and 0.01 fm^{-3}, respectively. In Figs. 3(a), 3(b), and 3(c), the symmetry free energies per nucleon in the LSM (thick black lines) and the SMF (thin blue lines) are compared at the three densities at different temperatures. As seen in Fig. 3(a) at $T =$ 2 MeV, at the lowest density, the two calculations yield nearly the same results; with increasing density, the difference in the two model predictions shows up prominently because of the formation of larger clusters in the SMF. This difference washes out gradually with increasing temperature and the results are not discernible as seen in Figs. 3(b) and 3(c). In Fig. 3(d), the symmetry free energies at $T = 2$ MeV for the three densities from the SNC (thick magenta lines) and MF (thin cyan lines) models are compared. In the liquid-drop mass formula, the symmetry energy is taken to be linear in X^2. This is seen to be nearly true also for symmetry free energy of nuclear matter in a density region around the saturation density [11] in the MF model; we find the same for dilute nuclear matter as is shown in Fig. 3(d). The symmetry energies can then be written as

$$e_{\rm sym} = C_E X^2, \quad f_{\rm sym} = C_F X^2, \tag{17}$$

where C_E and C_F are the symmetry energy and symmetry free energy coefficients. Clusterization affects this linearity at low temperatures; as the temperature is increased, the linearity tends to be restored as seen from Figs. 3(b) and 3(c). The symmetry energy has a similar behavior and is not shown here.

One interesting result that is borne out of the SMF calculation is that at a given T and ρ, asymmetric nuclear matter may become more stable than symmetric matter [$f(X) < f(0)$]. This may result in negative $f_{\rm sym}$ as is shown in Fig. 3(a). This happens at relatively higher densities. We find it to be because of the absence of isospin-conjugate (mirror) nuclei because of Coulomb interaction. Restricting the sum in Eq. (3) to only mirror nuclei removes this negativity. In the SNC model, clusters always occur in isospin-conjugate pairs; $f_{\rm sym}$ is then always positive as seen from Fig. 3(d).

The symmetry entropy per baryon, defined as $s_{\rm sym} = s(X) - s(0)$ is presented as a function of asymmetry for different densities and temperatures in Fig. 4. The notations used are the same as those used for Fig. 3. Comparison between the MF and the SNC models at the three densities is displayed in Figs. 4(b) and 4(d). In the MF model, the symmetry entropy decreases with asymmetry. This is akin to the *entropy of mixing*. The entropy per nucleon of an ideal two-component nucleon gas is given, from Gibbs-Duhem relation, by

$$s(X) = \frac{5}{2} - \frac{\rho_n}{\rho} \ln \zeta_n - \frac{\rho_p}{\rho} \ln \zeta_p. \tag{18}$$

Using the fact that for low density nucleonic matter

$$\rho_{n,p} \simeq \frac{2}{\lambda^3} \zeta_{n,p}, \tag{19}$$

the symmetry entropy can be shown to behave as

$$s_{\rm sym}(X) = -\tfrac{1}{2} X^2 \left(1 + \tfrac{1}{6} X^2 + \cdots\right), \tag{20}$$

which for low values of asymmetry decreases linearly with X^2. This is independent of both temperature and density and

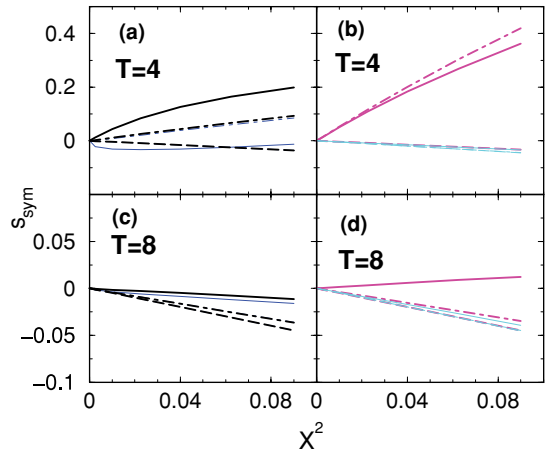

FIG. 4. (Color online) The symmetry entropy $s_{\rm sym}$ as a function of X^2 at different temperatures and densities. The notations are the same as described in the caption to Fig. 3.

is nearly manifested for the low density nuclear matter we have considered. As can be seen from the comparison with the SNC calculations, clusterization changes this behavior; in the density and temperature domain where clusterization becomes important, the symmetry entropy is larger compared to that in the MF model and can even be positive. In Figs. 4(a) and 4(c), comparison is made between the results from LSM and SMF. At high temperatures and low densities, the difference in the results from these models is not discernible; however, at relatively high density and low temperature, $s_{\rm sym}$ in the LSM is appreciably larger than that in the SMF as displayed in Fig. 4(a) for $\rho = 0.01$ fm^{-3} and $T = 4$ MeV. This is attributed to the relatively rapid growth of multiplicity (mostly of neutrons at the cost of p, He^3, and α) in the LSM model compared to that in the SMF model.

The conventional definition of the symmetry coefficients C_E and C_F as given by Eq. (17) holds good when $e_{\rm sym}$ and $f_{\rm sym}$ are linear or nearly linear in X^2. In Fig. 5, we display these symmetry coefficients as a function of density for temperatures

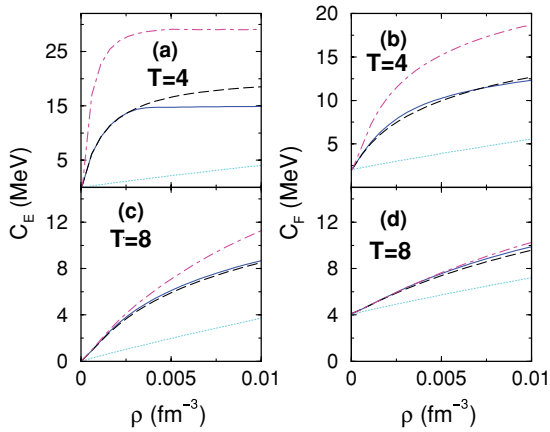

FIG. 5. (Color online) The symmetry coefficients C_E and C_F as a function of density at different temperatures in the models of mean field (dotted cyan), LSM (dashed black), SNC (dot-dashed magenta), and SMF (solid blue).

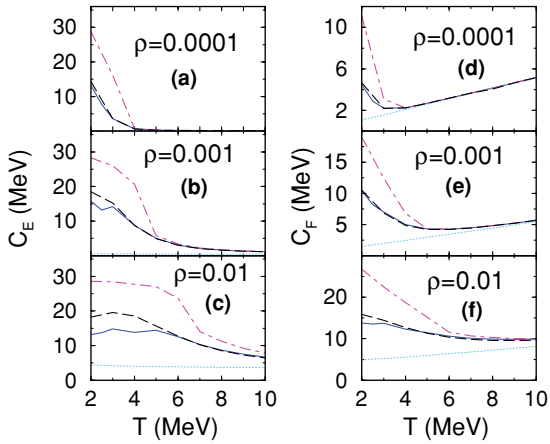

FIG. 6. (Color online) The symmetry coefficients C_E and C_F displayed as a function of temperature at densities $\rho = 0.0001, 0.001$, and 0.01 fm^{-3}. The notations are the same as described in the caption to Fig. 5.

when the symmetry energies are nearly linear in X^2 in the different models. In the density region investigated, in the MF model, the symmetry coefficients increase linearly with density in contrast to a power-law dependence $\sim(\rho/\rho_0)^\gamma$ with $\gamma \sim 0.7$ at relatively higher densities [28]. The symmetry coefficients are enhanced significantly when clusterization is considered. This is most prominent in the SNC model (dot-dashed lines), where, as already stated, at lower temperatures and higher densities the system is more liquid-like; this is reflected in the value of C_E in Fig. 5(a), which at higher densities saturates to $\sim$28 MeV, the value for normal nuclear matter as given in the liquid-drop mass formula we use [26]. The symmetry coefficients C_E in the LSM and SMF models are close at high temperature $T = 8$ MeV, but differ at $T = 4$ MeV where clusterization is more important. This difference is filled up for symmetry free energy coefficient C_F due to the symmetry free entropy [shown in Fig. 4(a)] resulting in practically the same C_F in both the models.

The temperature dependencies of the symmetry coefficients C_E and C_F at a few densities in all the models considered are displayed in the left- and right-hand panels of Fig. 6, respectively. In the mean-field model, shown by the dotted lines, C_E is linear and approximately constant for a given density as seen earlier [28]. At very low density $\rho = 0.0001$ fm^{-3}, it is nearly zero and not discernible in the figure. In the condensation models a pronounced increase in the values of C_E is observed, particularly at low temperatures. In the SNC model this value is close to that for normal nuclear matter as expected. At larger temperatures, values of C_E obtained in the condensation models approach those calculated from the MF model.

The symmetry free energy coefficient C_F, by our choice, can be written as

$$C_F = C_E - T\frac{s_{\rm sym}}{X^2}. \tag{21}$$

For dilute nuclear matter, in the MF model, C_E is linear in T at a particular density and $s_{\rm sym}$, as stated earlier, is negative and proportional to X^2. A linear increase of C_F with temperature is therefore expected in the mean-field model, which is realized as displayed by the dotted lines in the right-hand panels of Fig. 6. At higher temperatures, results for C_F in all the models tend to merge, particularly at low density because of the hindrance to form clusters. At lower temperatures, C_F is significantly higher with clusterization compared to that in the MF model. In Eq. (21), the first term on the right-hand side decreases with temperature whereas the second term increases with condensation; this interplay causes a minimum in C_F that is more pronounced at lower densities.

IV. CONCLUDING REMARKS

The role of condensation on some properties of dilute nuclear matter, namely, the nuclear EOS, the symmetry free energy, the symmetry entropy, and the symmetry coefficients, has been addressed in this article in the S-matrix framework. This approach has the advantage that the relevant observables can be directly connected to the experimentally measured quantities like the nuclear binding energies and the scattering phase-shifts. This approach contains no interaction potential parameters and, hence, the results are mostly model independent.

Except at very low densities, the nuclear EOS in the S-matrix approach differs appreciably from the one obtained in the MF model. The MF model, supplemented with Maxwell's construction, displays a liquid-gas phase transition on isothermal compression; in the S-matrix approach, the system responds to the compression by a marked growth of clusters out of the dilute nucleonic gas. The growth is hindered with isochoric heating.

One of the very remarkable features of the results on symmetry energies (both $e_{\rm sym}$ and $f_{\rm sym}$) in the SMF model is that the symmetry energies are generally nonlinear in X^2, contrary to the results in the MF model. The symmetry energies may even be negative in the SMF model at low temperatures, high densities, and small X. The symmetry entropy similarly displays a subtle behavior with clusterization. In the conventional definition, at a particular temperature and density, the symmetry coefficients are then no longer independent of the asymmetry parameter and may be negative. In the region where the symmetry energies are practically linear in X^2, the symmetry energy and free energy coefficients in the S-matrix approach are found to be appreciably larger compared to those obtained in the MF model. The nuclear EOS and the symmetry energies and coefficients are thus seen to have a significant dependence on the many-nucleon correlations or cluster formation in the low density nuclear matter. Inclusion of these effects are thus warranted for the study of physical phenomena like supernova dynamics that depend sensitively on the symmetry energy and its temperature and density dependence.

ACKNOWLEDGMENT

The authors acknowledge support from the Department of Science & Technology, Government of India.

[1] A. W. Steiner, M. Prakash, J. M. Lattimer, and P. J. Ellis, Phys. Rep. **411**, 325 (2005).
[2] B. A. Brown, Phys. Rev. Lett. **85**, 5296 (2000).
[3] C. J. Horowitz and J. Piekarewicz, Phys. Rev. Lett. **86**, 5647 (2001).
[4] A. S. Botvina, N. Buyukcizmeci, M. Erdogan, J. Lukasik, I. N. Mishustin, R. Ogul, and W. Trautmann, Phys. Rev. C **74**, 044609 (2006).
[5] M. B. Tsang *et al*., Phys. Rev. Lett. **92**, 062701 (2004).
[6] L. W. Chen, C. M. Ko, and B. A. Li, Phys. Rev. Lett. **94**, 032701 (2005).
[7] G. A. Souliotis, A. S. Botvina, D. V. Shetty, A. L. Keksis, M. Jandel, M. Veselsky, and S. J. Yennello, Phys. Rev. C **75**, 011601(R) (2007).
[8] D. V. Shetty, S. J. Yennello, and G. A. Souliotis, Phys. Rev. C **76**, 024606 (2007).
[9] B. A. Li, L. W. Chen, and C. M. Ko, Phys. Rep. **464**, 113 (2008), and references therein.
[10] C. Fuchs and H. H. Wolter, Eur. Phys. J. A **30**, 5 (2006).
[11] J. Xu, L. W. Chen, B. A. Li, and H. R. Ma, Phys. Rev. C **75**, 014607 (2007).
[12] S. K. Samaddar, J. N. De, X. Viñas, and M. Centelles, Phys. Rev. C **78**, 034607 (2008).
[13] B. Friedman and V. R. Pandharipande, Nucl. Phys. **A361**, 502 (1981).
[14] G. Peilert, J. Randrup, H. Stocker, and W. Greiner, Phys. Lett. **B260**, 271 (1991).
[15] H.-Th. Janka, K. Langanke, A. Marek, G. Martínez-Pinedo, and B. Müller, Phys. Rep. **442**, 38 (2007).
[16] C. J. Horowitz and A. Schwenk, Nucl. Phys. **A776**, 55 (2006).
[17] S. Kowalski *et al*., Phys. Rev. C **75**, 014601 (2007).
[18] R. Dashen, S.-K. Ma, and H. J. Bernstein, Phys. Rev. **187**, 345 (1969).
[19] S. Mallik, J. N. De, S. K. Samaddar, and Sourav Sarkar, Phys. Rev. C **77**, 032201(R) (2008).
[20] A. Bohr and B. R. Mottelson, *Nuclear Structure* (W. A. Benjamin, Inc., New York, 1969), Vol. I.
[21] R. Dashen and R. Rajaraman, Phys. Rev. D **10**, 694 (1974).
[22] R. Dashen and R. Rajaraman, Phys. Rev. D **10**, 708 (1974).
[23] E. Beth and G. E. Uhlenbeck, Physica **4**, 915 (1937).
[24] E. O'Connor, D. Gazit, C. J. Horowitz, A. Schwenk, and N. Barnea, Phys. Rev. C **75**, 055803 (2007).
[25] J. N. De and S. K. Samaddar, Phys. Rev. C **76**, 044607 (2007).
[26] W. D. Myers and W. J. Swiatecki, Nucl. Phys. **81**, 1 (1966).
[27] W. D. Myers and W. J. Swiatecki, Nucl. Phys. **A601**, 141 (1996); Lawrence Berkeley Laboratory Report LBL-36803.
[28] S. K. Samaddar, J. N. De, X. Vinas, and M. Centelles, Phys. Rev. C **76**, 041602(R) (2007).